WILEY ONLINE LIBRARY EarlyView publication on wileyonlinelibrary.com
(issue and page numbers not yet assigned;
citable using Digital Object Identifier – **DOI**)

Phys. Status Solidi B, 1–7 (2013) / **DOI** 10.1002/pssb.201248379

physica status solidi b
www.pss-b.com
basic solid state physics

Formation of the magnetic fractal structure in Co–SiO_2 granular nanocomposite system at percolation threshold

E. B. Dokukin[1], R. V. Erhan[*,1,2], A. Kh. Islamov[1], M. E. Dokukin[3], N. S. Perov[3], and E. A. Gan'shina[3]

[1] Frank Laboratory of Neutron Physics, Joint Institute for Nuclear Research, 141980 Dubna, Russia
[2] Horia Hulubei National Institute for Research and Development in Physics and Nuclear Engineering, MG-6, 077125 Bucharest-Magurele, Romania
[3] Faculty of Physics, Moscow State University, Leninskie Gory, Moscow 119992, Russia

Received 15 August 2012, revised 6 December 2012, accepted 27 March 2013
Published online 25 April 2013

Keywords composites, fractals, magnetic properties, nanoparticles, small-angle neutron scattering

[*] Corresponding author: e-mail erhan@nf.jinr.ru, Phone: +7-49621-62690, Fax: +7-49621-65882

Magnetic and structural properties of $(Co)_x(SiO_2)_{1-x}$ nanocomposite systems have been investigated over a wide range of Co concentrations using small-angle neutron scattering in combination with magnetic, magneto-optic, and magneto-transport characterization. It was found that in the region of structural percolation $(x = 0.46...0.6)$, the characteristics of magnetically correlated clusters are several times larger than the structural size of Co granules. Starting from the percolation point, the spatial distribution of magnetic nanoclusters can be described by the surface fractal model. With further growth of cobalt concentration $x \geq 0.67$ the formation of three-dimensional (3D) magnetic domains with typical sizes of 1.5 μm was observed.

1 Introduction Composite materials based on nanoparticles of magnetic metals dispersed in the nonmagnetic matrix are of great interest not only for fundamental study, but also for its possible applications. Physical properties of such composites can be diametrically opposite to the properties of original bulk materials. Composite materials have unique characteristics like giant magnetoresistance, giant tunnel magnetoresistance [1], and the giant anomalous Hall effect [2]. Moreover, the typical granular systems show featured behavior in linear and nonlinear optical and magneto-optical (MO) experiments [3, 4]. Nowadays MO properties of granular alloys are studied because of possible application as magneto-active recording media and wide range MO sensors. Recently it was suggested that granular alloys could be used as MO elements in magneto-photon crystals [5]. It has been shown, that magneto-transport and, especially, MO effects are sensitive not only to characteristic dimensions, shape and topology of granules, but also to variations in their magnetic or electronic structure [6]. Analysis of the magnetic interaction of granules and the clusters they form is very important for a correct explanation of the observed properties of granular nanocomposites.

A lot of research has been done to analyze the magnetic and topology dimensions of magnetic component in nanocomposite films. For example, by analyzing magnetization curves it was found that structural and magnetic sizes of the granules practically coincide below the percolation threshold, but as the percolation threshold is being approached a slight increase in the average magnetic size was observed for an almost unchanged structural granules size [7]. However, as soon as the geometric percolation threshold is reached, the determination of the magnetic size of the granules or clusters by means of magnetization curves becomes incorrect and, therefore, the analysis can be done only for system with magnetic material concentration up to 55 at%. At the same time, correct determination of the magnetic structure near and above the percolation threshold region is crucial for the calculation of magnetic and MO properties of composites.

In this work the structural and magnetic sizes of magnetic metal granules in $(Co)_x(SiO_2)_{1-x}$ nanocomposite films were measured using small-angle neutron scattering. The dependence of the structural and magnetic properties on the magnetic metal concentration was studied for the most

interesting interval of x ($x = 0.4...0.72$). The results collected using neutron scattering, magneto-optic, magneto-static, and magneto-transport techniques were compared.

2 Materials and methods The magnetic nanocomposite samples of $(Co)_x(SiO_2)_{1-x}$ were prepared using ion-beam deposition in argon atmosphere. The samples were grown on single crystal silicon substrates. The temperature of substrates during deposition was kept at 300 K. The samples thickness was from 125 μm up to 135 μm, the concentration of cobalt ($\underline{x}$) ranged from $x = 0.4$ up to $x = 0.72$. The average size of metallic granules changes from 2 to 6 nm with increasing of metal concentration in the sample [8].

Magnetostatic measurements were performed using a vibration sample magnetometer in a maximum magnetic field up to 15 kOe at room temperature. Square samples with a size of 7–10 mm were used. Magneto-transport properties were measured in the magnetic field of up to 16 kOe at temperatures 295 and 77 K. All magneto-transport measurements were performed using the two-point probe method with samples 7–10 mm length and 2 mm width. During magneto-transport measurements the external magnetic field was applied perpendicularly to the sample plane. In order to measure the MO properties of the sample, the Kerr effect in the transversal geometry [transversal Kerr effect (TKE)] was used. The TKE spectra were measured over the incident light energy interval E of 1–3 eV using an automated MO spectrometer. A dynamic method was used. The amplitude of the applied alternating magnetic field was up to 3.5 kOe. Such method allows the detection of relative change in intensity of the reflected linearly polarized light with a precision of up to 10^{-5} and with a maximum error of ≈5%. The MO measurements were conducted at room temperature.

Small-angle neutron scattering measurements of the Co–SiO_2 systems were performed on the time-of-flight spectrometer YuMO at the reactor IBR-2M in FLNP, JINR (Dubna, Russia) [9]. In the spectrometer, detectors were situated at 5.28 and 13.04 m from the sample hence, the momentum transfer interval was from 0.007 to 0.25 $Å^{-1}$. The diameter of the sample in the beam was 14 mm. The measurements were performed at 293 K in a zero external magnetic field. The measured neutron scattering spectra were corrected for the transmission and thickness of the sample, background scattering on the film substrate and on the vanadium reference sample [10].

3 Results and discussion It is known that MO response of nanocomposites is very sensitive to changes of their microstructure and thus allows to determine the concentration of ferromagnetic metal that corresponds to the percolation threshold [11, 12]. Here the TKE was used to find the cobalt concentration corresponded to the percolation threshold in the Co–SiO_2 system. On spectral and concentration dependencies of TKE presented in Fig. 1 the maximum of the MO signal is clearly seen in the near infrared range of spectra (for the incident light energies from 1.25 to 1.42 eV) for cobalt concentrations of $x = 0.44$–0.51,

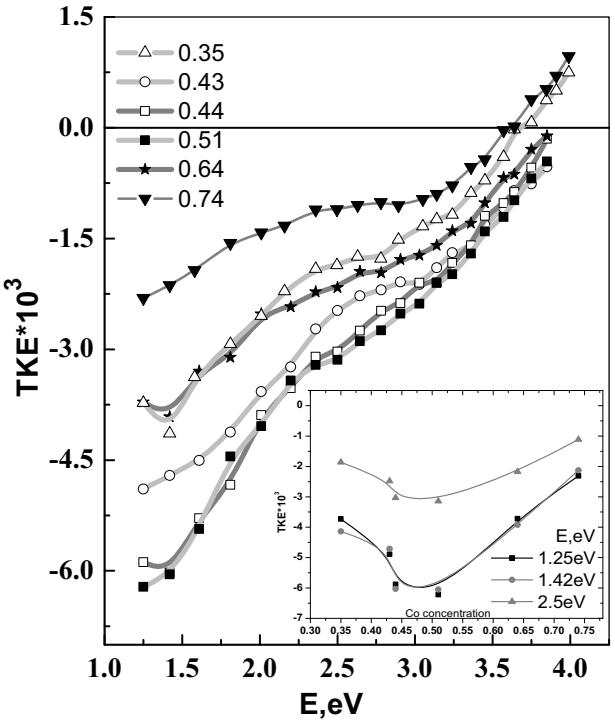

Figure 1 The spectral dependence of TKE for $Co_x(SiO_2)_{1-x}$ with different Co concentration; inset: concentration dependence of TKE for the light energy of 1.25, 1.42, and 2.5 eV.

which points to the presence of percolation threshold in this concentration range [13]. The presence of the percolation threshold at the Co concentration of $x = 0.45 - 0.51$ was also indirectly confirmed by magnetostatic measurements. As one can see from Fig. 2 for Co concentrations above $x = 0.51$ the coercive field (H_c) shows sharp nonlinear growth which can be explained by formation of ferromagnetic clusters in the sample and therefore presence of the percolation threshold.

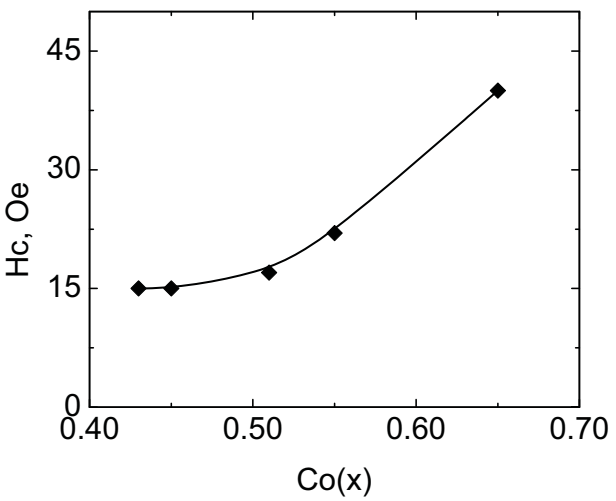

Figure 2 The coercivity as a function of Co concentration.

3.1 Magnetoresistance Figure 3 shows the dependence of the relative magnetoresistance on external magnetic field. Here R_H and R_0 are the resistances with and without applied external magnetic field, respectively. The measurements were performed at 77 and 295 K for different cobalt concentrations below and above the percolation threshold. The maximum magnetoresistance effect at room temperature reaches 2%, and at 77 K it was up to 4.5%. This is a typical magnetoresistance for such granular structures [14, 15].

As it is seen from the curves in Fig. 3 the two competing mechanisms of magnetoresistance are presented. The first one is connected to the metallic conductivity of the granulars and leads to the positive magnetoresistance. The second relates to the magnetic moments disorientation that resulting in negative contribution (similar to giant magnetoresistance). At small magnetic field, the main contribution appears from the mechanism of positive magnetoresistance because of the small change of orientation of the magnetic moment of Co clusters due to their large anisotropy field. When the external magnetic field is large enough to change the granular magnetization and their magnetic moments become parallel, the resistance decreases [16].

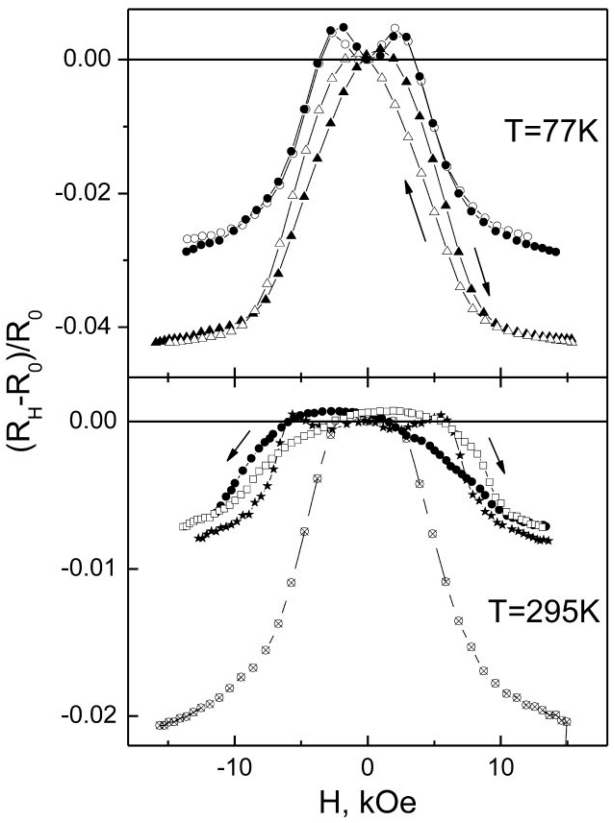

Figure 3 The relative magnetoresistance $(R_H - R_0)/R_0$ for $(Co)_x(SiO_2)_{1-x}$ at 77 K (upper) [for ○ $x = 0.43$ and △ $x = 0.65$ magnetic field changes from +16 to −16 kOe; for ● $x = 0.43$ and ▲ $x = 0.65$ magnetic field changes from −16 to +16 kOe] and at 295 K (bottom) [★ $x = 0.43$; ⊗ $x = 0.51$; for ● $x = 0.70$ magnetic field changes from +16 to −16 kOe; for □ $x = 0.70$ magnetic field changes from −16 to +16 kOe].

It is interesting to note, that below the electric percolation threshold a decrease in temperature leads to an increase in the positive magnetoresistance in low magnetic fields, and above percolation threshold – to an increase in the negative magnetoresistance. Such behavior can be explained by the fact that below the percolation threshold the existing magnetic granules which are not forming magnetic clusters could participate in conductivity. The magnetic moment of these granules could reverse its direction in a small magnetic field. This does not significantly affect the magnetoresistance, but influence the magnetization behavior (see Fig. 2).

4 Small-angle neutron scattering studies of $(Co)_x(SiO_2)_{1-x}$ films $(Co)_x(SiO_2)_{1-x}$ is a paramagnetic system which consists practically from uniformly magnetized particles in nonmagnetic matrix with an isotropic microstructure (randomly orientated spins). In the absence of external magnetic field their magnetization appears to be in average zero – so called super paramagnetic state.

In the case of an unpolarized incident neutron beam and in absence of applied magnetic field the intensity of small-angle neutron scattering is given by [17]:

$$I(Q) = I(Q)_{\text{nuc}} + \frac{2}{3} I(Q)_{\text{mag}}. \tag{1}$$

Nuclear and magnetic scattering intensities from Co granules being in a SiO_2 matrix with size distribution given by Gaussian law, neglecting inter-particle correlations, can be written as

$$I_{\text{nuc}}(Q) = \int_0^\infty N_1(R) N_0 \left(\rho_{\text{Co}} - \rho_{\text{SiO}_2}\right)^2 V_{\text{nuc}}^2 F_{\text{nuc}}^2 \mathrm{d}R, \tag{2}$$

$$I_{\text{mag}}(Q) = \int_0^\infty N_2(R) N_0 \rho_{\text{mag}}^2 V_{\text{mag}}^2 F_{\text{mag}}^2 \mathrm{d}R, \tag{3}$$

$$N_1(R) = \frac{\exp\left(-\left(\frac{R_{\text{Co}}-R}{\sqrt{2}\sigma_1}\right)^2\right)}{\sqrt{2\pi}\sigma_1},$$

$$N_2(R) = \frac{\exp\left(-\left(\frac{R_{\text{mag}}-R}{\sqrt{2}\sigma_2}\right)^2\right)}{\sqrt{2\pi}\sigma_2}, \tag{4}$$

$$N_0 = \frac{\varphi_{\text{Co}} V_{\text{tot}}}{\int_0^\infty N_1(R) V \mathrm{d}R},$$

$$\varphi_{\text{Co}} = \frac{x}{x + (1-x)\frac{\nu_{\text{Co}}}{\nu_{\text{SiO}_2}}}, \tag{5}$$

$$V = \frac{4}{3}\pi R^3,$$

$$F = 3\frac{\sin(QR) - (QR)\cos(QR)}{(QR)^3}, \tag{6}$$

where φ_{Co} is the volume part of Co nanoparticles in $(Co)_x(SiO_2)_{1-x}$ matrix, $V_{\text{tot}} = \pi \frac{D^2}{4} T = 1.9 \times 10^{-2}\text{cm}^3 \times 0.0125$ cm is the total volume of the sample in-beam and

ν_{Co} and ν_{SiO_2} are the partial volumes of Co and SiO_2; $\rho_{Co} = 2.274 \times 10^{10}\text{cm}^{-2}$ and $\rho_{SiO_2} = 4.192 \times 10^{10}\text{cm}^{-2}$ are the nuclear scattering densities of Co and SiO_2, respectively; $\rho_{mag} = 4.14 \times 10^{10}\text{cm}^{-2}$ is the magnetic scattering density of Co [18], R_{Co}, R_{mag} are the average radii of cogranules and its magnetic parts. There are four fitting parameters R_{Co}, R_{mag} and σ_1, σ_2. The intensities at zero angles were calculated using Eqs. (2)–(6). The relative scaling factor between experimental and theoretical curves was not used.

The resolution of YuMO time of flight small-angle scattering instrument ($\Delta Q/Q$) varies from 5 to 18% for Q ranging from 0.3 to 0.005 Å^{-1}. The effect of resolution at high Q is insignificant. A change of sphere radius $R = 18$ Å with addition of resolution changes value of the radius on 0.2 Å.

Figure 4 shows the scattering curve from $(Co)_x(SiO_2)_{1-x}$ at $x = 0.41$ and 0.46. The fitting of the experimental data using Eqs. (2)–(6) gives average $R_{Co} = 23.5$ Å, $R_{mag} = 18$ Å and dispersions $\sigma_1 = \sigma_2 = 3$ Å with $\chi^2 = 1.3$ (Fig. 4, solid line). If the same radiuses for magnetic and structural sizes of Co granules were used the radiuses values are $R_{Co} = R_{mag} = 18$ Å and $\chi^2 = 3.3$ (Fig. 4, dotted line). Polydispersivity of granules is sufficiently small and is about $\sqrt{2}\sigma/R_{Co} \approx 20\%$. As one can see that the difference between structural and magnetic radiuses is about 5.5 Å. It might result in small sizes of nanoparticles and as consequence a high curvature with nonmagnetic amorphous surface layer. A similar behavior was reported in Refs. [18, 19].

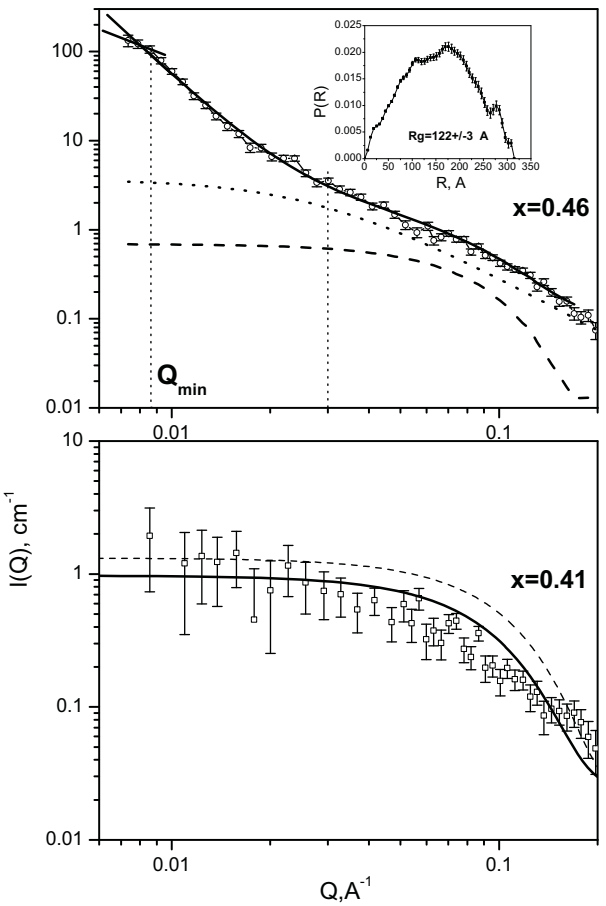

Figure 4 The intensity of small-angle neutron scattering of $(Co)_x(SiO_2)_{1-x}$ granular nanocomposite films at Co concentrations. Bottom figure for $x = 0.41$: □ experimental data; solid line: best fit with $R_{Co} = 23.5$ Å, $R_{mag} = 18$ Å, $\sigma_1 = \sigma_2 = 3$ Å with $\chi^2 = 1.3$; dotted line: model fit with $R_{Co} = R_{mag} = 18$ Å, $\sigma_1 = \sigma_2 = 3$ Å with $\chi^2 = 3.3$. Top figure for $x = 0.46$: ○ experimental data; dashed line: calculated nuclear scattering; dotted line: Ornstein–Zernike magnetic fluctuations; solid lines: Guinier and total neutron scattering, calculated from Eq. (7). In the inset, the pair distribution function $P(R)$ is presented.

The intensity $I(Q)$ changes cardinally for $x = 0.46$ (Fig. 4, top). A small change in the Co concentration by 0.05 results in a jump of intensity growth by two orders of magnitude at small Q. This can be explained by the occurrence of large scattering volumes due to the magnetic interactions. $I(Q)$ clearly shows three different regions of the scattering:

$$\begin{aligned} I(Q) &= I(0)e^{-\frac{R_g^2 Q^2}{3}}, && Q \le 0.0085\ \text{Å}^{-1} \\ I(Q) &= I_1(0)Q^{-\alpha}, && 0.0085\ \text{Å}^{-1} < Q \le 0.03\ \text{Å}^{-1} \\ I(Q) &= \frac{I_2(0)}{1+\xi_{mag}^2 Q^2} + I_{nuc}(Q), && 0.03\ \text{Å}^{-1} < Q \le 0.2\ \text{Å}^{-1}. \end{aligned} \tag{7}$$

The first interval ($Q \le 0.0085$ Å^{-1}) is described by the Guinier approximation with the gyration radius $R_g = 124 \pm 20$ Å. The second interval ($0.0085\ \text{Å}^{-1} < Q \le 0.03\ \text{Å}^{-1}$) shows a power law behavior of $I(Q) \approx Q^{-\alpha}$ with $\alpha = 3.43$. The scattering power law in terms of fractal model with $3 < \alpha < 4$ is typical for surface fractals – two-dimensional (2D) objects with rough surfaces [20].

The third interval ($0.03\ \text{Å}^{-1} < Q \le 0.2\ \text{Å}^{-1}$) is the region of short range nuclear and magnetic correlations [third and forth members in Eq. (7)]. Nuclear scattering was calculated from Eqs. (2)–(6) and the magnetic contribution was obtained from Ornstein Zernike equation, which describes the behavior of system near critical points where the fluctuations increase considerably.

The average radius of cobalt and standard deviation for $x = 0.46$ concentration are $R_{Co} = 23.5 \pm 1$ Å and $\sigma = 3$ Å as well as for $x = 0.41$, whereas the magnetic correlation length is $\xi = 35$ Å instead of $R_{mag} = 18$ Å for $x = 0.41$. Assuming that these granules form a primitive cubic lattice, it is possible to get the average parameter of the unit cell d from known R_{Co} and volume fraction φ_{Co}. And reverse, from known d and φ_{Co} to obtain the value of R_{Co}:

$$d^3 = \frac{\frac{4}{3}\pi R_{nuc}^3}{\varphi_{Co}}. \tag{8}$$

The calculated lattice parameters d for 0.41 and 0.46 Co concentrations are 68.2 and 64.5 Å, respectively. Therefore, the distances between Co granules are 21.2 Å for 0.41 and 17.5 Å for 0.46.

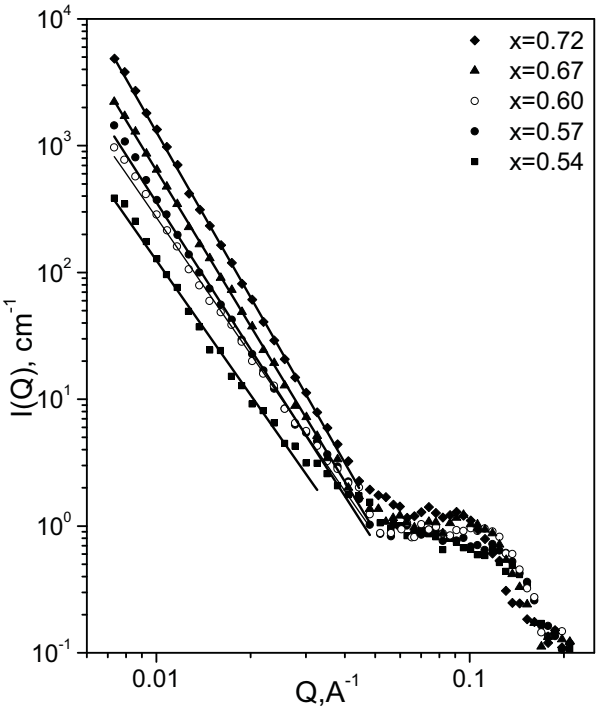

Figure 5 The intensity of small-angle neutron scattering from $(Co)_x(SiO_2)_{1-x}$ granular nanocomposite films at Co concentrations $x = 0.54, \ldots, 0.72$ with their model fits (■ 0.54, ● 0.57, ○ 0.60, ▲ 0.67, ▼ 0.72).

At $x = 0.41$ $d = 68.2$ Å $\geq 2R_{mag} = 36$ Å, while for 0.46 the magnetic correlation length exceeds the average lattice parameter $2\xi = 70$ Å $\geq d = 64.5$ Å. It means that Co granules interact with each other and form magnetically correlated clusters.

To estimate the linear size of 2D magnetic clusters at 0.46 concentration we used the relation between gyration radius $R_g = 124 \pm 20$ Å and the parameters of the disc: radius R and thickness T, where $T \ll R$, $R_{rmg}^2 = \frac{R^2}{2} + \frac{T^2}{12}$ [21]. Supposing that the thickness of one layer of $(Co)_x(SiO_2)_{1-x}$ is about $T \approx 60$ Å, we obtain the linear size of 2D clusters $L = 2R \approx 340$Å. Similar results were obtained by the use of the indirect Fourier transform program GNOM [22], that evaluates the particle distance distribution function $p(r)$ and the radius of gyration R_g. This method gives the maximal size of the cluster ≈325 Å and radius of gyration $R_g = 122$ Å.

The intensities of small angle neutron scattering $I(Q)$ of $(Co)_x(SiO_2)_{1-x}$ films $x = 0.54..0.72$ are shown in Fig. 5. In the Q range from 0.007 to 0.05 Å^{-1} the scattering intensity shows a power law behavior similar to the scattering from the surface fractals up to $x = 0.6$ (as can be seen from Table 1).

The systems where the structure of the metal plase behaves as a fractal belong typically to the systems where both components are ''unwettable'' *e.g.*, Co–SiO_2 or Ni–SiO_2 [23].

IN the high Q region from 0.06 to 0.2 Å^{-1} the correlation peak appears instead of Ornstein-Zernike magnetic fluctuations. The peak position $d = 2\pi/Q_{peak}$ corresponds to the mean distance between Co granules and the average radius of Co particles can be obtained from Eq. (8). With Co concentration growth the height of peak slightly increases and d changes from 62 to 67 Å (see Table 1). Accordingly, R_{Co} obtained from d and known φ_{Co} increase from 23.5 to 31.5 Å. The growth of Co granules can be explained by the technological factor, *i.e.*, manufacturing of the samples with higher cobalt concentration leads to the increase of the granule sizes. The correlation peak on the scattering curve and reasonable results obtained using Eq. (8) (see Table 1) indicate that the majority of cobalt granules are still separated by SiO_2 layer.

With the increase in Co concentration up to $x = 0.57$, the index α and the scattering intensity also increases monotonously as $Q \to 0$, which confirms that the volumes with the same magnetization direction are growing and the magnetic–nonmagnetic region boundary is getting less rough.

The only exception was observed near the Co concentration of $x = 0.6$ where intensity ($I(0.007$ Å$^{-1})$) of the neutron scattering decreased by 1.5 times in comparison with the smaller concentration of $x = 0.57$ (see Fig. 5). Moreover, the index α decreases from 3.85 to 3.58. Such nonmonotonic behavior of the fractal dimensionality and scattering intensity in the region around $x = 0.6$ leads to the change

Table 1 The parameters of the $(Co)_x(SiO_2)_{1-x}$ films. R_{Co} and R_{mag} are the nuclear and magnetic radiuses of cobalt granules, φ_{Co} the volume fraction of cobalt in SiO_2 matrix, α the index of the exponential scattering function, d the position of the correlation peak corresponding to the average distance between cobalt particles, $I(0.007$ Å$^{-1})$ the intensity at minimal measured $Q = 0.007$ Å^{-1}, ξ the length of Ornstein–Zernike fluctuations, and L is the linear size of magnetic 2D cluster.

x_{Co}	φ_{Co}	α	d (Å)	$I(0.007$ Å$^{-1})$ (cm^{-1})	R_{mag} (Å)	R_{Co} (Å)
0.41	0.17	–	68.2 ± 1	1.3	$R_{mag} = 18 \pm 2$	23.5 ± 1
0.46	0.20	-3.43 ± 0.1	64.5 ± 1	134	$\xi = 35 \pm 3$, $L \approx 340$	23.5 ± 1
0.54	0.26	-3.53 ± 0.05	62 ± 2	385	–	24.5 ± 1
0.57	0.28	-3.85 ± 0.03	63 ± 2	1443	–	25.7 ± 1
0.60	0.31	-3.58 ± 0.03	63 ± 2	970	–	26.4 ± 1
0.67	0.38	-4.08 ± 0.03	64 ± 2	2215	$R_{mag} \approx 7500$	28.7 ± 1
0.72	0.42	-4.34 ± 0.02	67 ± 2	4858	–	31.5 ± 1

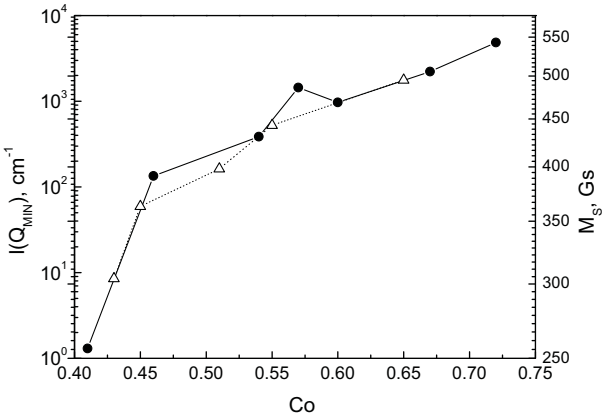

Figure 6 The small-angle neutron scattering intensity $I(Q_{\min})$ at minimal measured $Q = 0.007$ Å^{-1} (● left axis), and the saturation magnetization M_s (△ right axis) dependence on the Co concentration (x).

of the magnetic state of the cobalt film at this concentration. The decrease of scattering intensity is the result of reduction of the average volume of magnetic nanocluster or can be interpreted as that a part of the large 2D magnetic nanoclusters transforms to three-dimensional (3D) nanoclusters of smaller sizes.

Further increase in the cobalt concentration results in filling of fractal nanocluster voids and reducing the cluster surface. The scattering intensity at $x = 0.67$ follows to classical well-known Porod law with $\alpha = 4$ for 3D objects with smooth surfaces:

$$I(Q) = 2\pi \frac{2}{3} \rho_{\text{mag}}^2 Q^{-4} \frac{S}{V}. \tag{9}$$

To roughly estimates of the sizes of magnetic clusters it is possible to use the sphere model for which $\frac{S}{V} = \frac{3}{R}$. The obtained radius is equal to $R_{\text{mag}} \approx 7500$ Å.

For the concentration $x = 0.72$ the index α exceeds 4 and equals 4.34 — clusters with diffuse interface; where $I(q)$ goes as $q^{-(4+\beta)}$, and β describes the exponential decay of the diffuse interface [24]. Figure 6 presents the dependence of the magnetization saturation and the small-angle scattering intensity $I(0.007\ \text{Å}^{-1})$ on the Co concentration. It is seen that, above the percolation threshold ($x \gtrsim 0.45$) the scattering intensity for minimum Q and saturation magnetization growth obeys an exponential law. Such behavior additionally proves that small-angle scattering has net magnetic nature.

The behavior of scattering curves allows us to conclude that in the region of electric percolation transition ($x \approx 0.46..0.50$) the size of magnetic nanoclusters is several times larger than the characteristic structural size of Co granules. Furthermore, with an increase of metal concentration this difference reaches two orders of magnitude. This can be explained by the establishing of the exchange interaction between Co granules in the region of electric percolation. While the distance between the neighboring granules is lower than the tunneling threshold, (≈1.75 nm for SiO_2, neutron scattering experimental data) the exchange interaction between granules becomes possible and the tunneling magnetoresistance effects dominates over other effects.

At the same time, unlike systems where granules can get into a contact [25, 26] and form an extended metallic network near the percolation threshold, in the $(Co)_x(SiO_2)_{1-x}$ system the geometric percolation is not observed at maximum magnetoresistance ($x \approx 0.47$ metal content) and appears only around at $x = 0.57..0.6$.

This can be explained by the fact that in opposite to the structural percolation theory, the conductivity sets on earlier than the geometric percolation threshold is reached ($x < x_{\text{perc}}$). Such regime is called a dielectric regime [25, 26] where resistance decreases as a result of tunneling conductivity [27]. The onset of the phase transition at $x = 0.47$ and the geometric percolation transition at $x = 0.57..0.6$ is in good agreement with the theory of percolation transitions [28, 29]. For example, in Ref. [30] the authors also show that electric percolation appears earlier than the structural..

5 Conclusions Using neutron scattering, the formation of magnetic nanoclusters (with sizes from 3.5 to 35 nm) from the initially magnetically isolated cobalt granules was observed for the thin film granular of $(Co)_x(SiO_2)_{1-x}$ samples near electric percolation threshold ($x = 0.45 - 0.50$), found using TKE. It was shown that the magnetic granules in such magnetic nanoclusters behave as individual particles for cobalt concentrations up to $x = 0.72$, which can point to absence of the direct contact between granules. Starting from the electric percolation point, the structural hierarchy of the magnetic nanoclusters can be described by the fractal structure model. The formation of the "magnetic fractal" can define the general magnetic properties of composites and could be the reason of unique magnetoresistance properties near the electric percolation threshold where two competing mechanisms of magnetoresistance are observed. It was shown that the nonmonotonic behavior of the scattering intensity, saturation magnetization, and maximum of positive magnetoresistance observed in the region of $x = 0.57–0.60$ is linked to the transition of magnetic nanoclusters from the initial 2D arranged state to the formation of the large 3D magnetic "domains" with typical size of 1.5 μm.

Acknowledgements We would like to acknowledge the grant No. 71-01.02.2012-15 of the Plenipotentiary Representative of the Romanian Government at Joint Institute for Nuclear Research Dubna and theme No. 04-4-1069-2009/2014 at Frank Laboratory for Neutron Physics, Joint Institute for Nuclear Research Dubna.

References

[1] H. Fujimori, S. Mitani, and S. Ohnuma, Mater. Sci. Eng. B **13**, 219 (1995).
[2] A. Pakhomov, X. Yan, and Y. Xu, J. Appl. Phys. **79**, 6140 (1996).

[3] H. Akinaga, M. Mizuguchi, T. Manado, E. Ganshina, A. Granovsky, I. Rodin, A. Vinogradov, and A. Yurasov, J. Magn. Magn. Mater. **470**, Part I, 242–245 (2002).
[4] E. Gan'shina, M. Kochneva, M. Vashuk, A. Vinogradov, A. Granovsky, V. Gushchin, P. Shcherbak, Chong-Oh Kim, and Cheol Gi Kim, Phys. Met. Metallogr. **102**, (Suppl. 1), S32–S35 (2006).
[5] J. Boriskina, S. G. Erokhin, A. B. Granovsky, A. P. Vinogradov, and M. Inoue, Phys. Solid State **48**(4), 717. (2006).
[6] E. Gan'shina, A. Granovsky, B. Dieny, M. Kumaritova, and A. Yurasov, Physica B **299**, 260 (2001).
[7] K. Yakushiji, S. Mitani, K. Takanashi, J. G. Ha, and H. Fujimori, J. Magn. Magn. Mater. **212**, 75–81 (2000).
[8] O. V. Stognei, Y. E. Kalinin, A. V. Sitnikov, I. V. Zolotukhin, and A. V. Slyusarev, Phys. Met. Metallogr. **91**, 21–28 (2001).
[9] A. I. Kuklin, A. Kh. Islamov, and V. I. Gordeliy, Neutron News **16**, 16 (2005).
[10] Yu. M. Ostanevich, Macromol. Chem. Symp. **15**, 91 (1988).
[11] E. Gan'shina, K. Aimuta, A. Granovsky, M. Kochneva, P. Sherbak, M. Vashuk, K. Nishimura, and M. Inoue, J. Appl. Phys. **95**(11), 6882. (2004).
[12] E. Gan'shina, A. Granovsky, B. Dieny, M. Kumaritova, and A. Yurasov, Physica B **299**(3–4), 260 (2001).
[13] E. A. Gan'shina, M. V. Vashuk, A. N. Vinogradov, A. B. Granovsky, V. S. Gushchin, P. N. Shcherbak, Yu. E. Kalinin, A. V. Sitnikov, K. Chong-Oh, and K. Cheol Gi, J. Exp. Theor. Phys. **98**(5), 1027 (2004).
[14] M. Holdenried, B. Hackenbroich, and H. Micklitz, J. Magn. Magn. Mater. **231**, L13–L19 (2001).
[15] O. V. Stognei, Yu. E. Kalinin, I. V. Zolotukhin, A. V. Sitnikov, V. Wagner, and F. J. Ahlers, J. Phys.: Condens. Matter **15**, 4267–4277 (2003).
[16] U. Hartmann, Magnetic Multilayers and Giant Magnetoresistance: Fundamentals and Industrial Applications (Springer, Berlin, Heidelberg, New York, 2000).
[17] M. V. Avdeev, E. Dubois, G. Meriguet, E. Wandersman, V. M. Garamus, A. V. Feoktystov, and R. Perzynski, J. Appl. Crystallogr. **42**, 1009–1019 (2009).
[18] A. Wiedenmann, Physica B **297**, 226–233 (2001).
[19] A. Wiedenmann, U. Lemke, A. Hoell, R. Muller, and W. Schuppel, Nanostruct. Mater. 601–604 (1999).
[20] J. Teixeira, J. Appl. Crystallogr. **21**, 781–785 (1988).
[21] L. A. Feigin and D. I. Svergun, Structure Analysis by Small-Angle X-ray and Neutron Scattering (Plenum Press, New York, 1987), p. 335.
[22] D. I. Svergun, J. Appl. Crystallogr. **25**, 495–503 (1992).
[23] D. Toker, D. Azulay, N. Shimoni, I. Balberg, and O. Millo, Phys. Rev. B **68**, 041403(R) (2003).
[24] P. W. Schmidt, D. Avnir, D. Levy, A. Hohr, M. Steiner, and A. Roll, J. Chem. Phys. **94**, 1474–1479 (1991).
[25] B. Abeles, P. Sheng, M. D. Coutts, and Y. Arie, Adv. Phys. **24**, 407 (1975).
[26] B. Abeles, Appl. Solid State Sci. **6**, 1 (1976).
[27] J. H. Smuckler and P. Finnerty, Adv. Chem. Ser. **134**, 171 (1974).
[28] D. Y. Kim, H. J. Heermann, and D. P. Landau, Phys. Rev. B **35**, 3661 (1987).
[29] D. Stauffer and A. Aharony, Introduction to Percolation Theory (Taylor and Francis, London, 1992).
[30] A. Gerber, A. Milner, B. Groisman, M. Karpovsky, A. Gladkikh, and A. Sulpice, Phys. Rev. B **55**, 10 (1997).